fibers

MDPI

Article

Random Plasmonic Laser Based on Bismuth/Aluminum/Yttria/Silver Co-Doped Silica Fiber with Microcavity Shaped Tip

José Augusto de la Fuente León [1], Ma. Alejandrina Martínez Gámez [1,*], José Luis Lucio Martinez [2], Alexander V. Kir'yanov [1], Karim Gibrán Hernández Chahín [2] and Mukul Chandra Paul [3]

[1] Centro de Investigaciones en Óptica, Loma del Bosque 115, Col. Lomas del Campestre, León 37150, Mexico; augustofl@cio.mx (J.A.d.l.F.L.); kiryanov@cio.mx (A.V.K.)
[2] Laboratorio de Aplicaciones Cuánticas, División de Ciencias e Ingenierías del Campus León de la Universidad de Guanajuato, Loma del Bosque 103, Col. Lomas del Campestre, León 37150, Mexico; pplucio@gmail.com (J.L.L.M.); karim.gibran.hernandez.chahin@cern.ch (K.G.H.C.)
[3] Fiber Optics and Photonic Division, Central Glass and Ceramic Research Institute, 196, Raja S.C. Mullick Road, Kolkata 700032, India; paulmukul@hotmail.com
* Correspondence: mamg@cio.mx

Abstract: In this study, we demonstrate a proof of principle of an all-fiber random laser due to the plasmonic effect. This was achieved with a fiber co-doped with bismuth/aluminum/yttria/silver in which a microsphere (microcavity) at the fiber's tip was made using a splicing machine. The presence of bismuth and silver nanoparticles in the fiber along with bismuth–aluminum phototropic centers stands behind the observed phenomenon. The effect can be attributed to the in-pair functioning of this unit as an active medium and volumetric plasmonic feedback, resulting in lasing at 807 nm under 532 nm pumping with a notably low (~2 mW) threshold.

Keywords: random fiber laser; bismuth; nanoparticles; surface plasmon resonance

check for updates

Academic Editors: Andrey Pryamikov and Martin J. D. Clift

Received: 1 October 2024
Revised: 16 January 2025
Accepted: 22 January 2025
Published: 5 February 2025

Citation: de la Fuente León, J.A.; Martínez Gámez, M.A.; Lucio Martinez, J.L.; Kir'yanov, A.V.; Hernández Chahín, K.G.; Paul, M.C. Random Plasmonic Laser Based on Bismuth/Aluminum/Yttria/Silver Co-Doped Silica Fiber with Microcavity Shaped Tip. *Fibers* **2025**, *13*, 17. https://doi.org/10.3390/fib13020017

Copyright: © 2025 by the authors. Licensee MDPI, Basel, Switzerland. This article is an open access article distributed under the terms and conditions of the Creative Commons Attribution (CC BY) license (https://creativecommons.org/licenses/by/4.0/).

1. Introduction

Since their first emergence in 1994 by Lawandy et al. [1] and De Matos et al. [2], interest in random lasers (RL) and, particularly, random fiber lasers (RFL) has increased considerably. This interest mostly stemmed from the identification of materials with properties that have potentials in RL/RFL production, such as conjugated polymer films [3], laser dye molecules [4], organic dye-doped gel films [5,6], dielectric materials [7–10], and metallic nanoparticles (NPs). RL/RFL offers such advantages as low cost, simplicity of fabrication, and potential applicability in versatile areas, e.g., in optical engineering [11–13], biomedical diagnostics [14], lighting technologies [15], optical astronomy, microscopy [8,16], etc. Meanwhile, the major challenges for these devices are pump threshold reduction and possible miniaturization. Researchers can refer to a recent review of the state-of-the-art of RFL [17].

The gain in RL/RFL is produced within an active medium that is basically featured by high scattering, caused by NPs. In this sense, the use of metal NPs, e.g., bismuth (Bi) NPs, has become relevant in the field because metallic inclusions exhibit optical properties different from those exhibited by bulk materials [18,19]. It is known that if electromagnetic radiation at a proper wavelength is incident on metallic NPs, it promotes localized surface plasmon resonance (SPR) [20], which in turn leads to strong light scattering, resonant optical absorption, and increment of electric field strength in the vicinity of the NP's surface.

Meanwhile, on the one hand, over the past few years, the use of Bi-doped fibers (BDF) towards the development of amplifiers and lasers on their base has shown significant

progress. However, most of the research with BDF was focused on obtaining gain/lasing in the 'windows' of the near-infrared (NIR) region, uncoverable with fibers doped with rare earths but easily accessible with BDF due to inherent Bi-active centers (BAC) (see, e.g., [21–24]). On the other hand, in a few reports [25–30] it was revealed that co-doping of glasses with rare earth and silver (Ag) NPs can improve the fluorescence potential of the former. The ground behind the effect is the overlap of the Ag-NPs SPR's peaks with the absorption or fluorescence bands of the rare-earth ions (see, e.g., [31–35]).

Bearing the above information in mind, we attempted (and were successful) to fabricate silica fiber co-doped with Bi and Ag (hereafter—'BAYAg fiber') with the aim of exploring the combinative potential of BAC (for lasing) and Bi-NP/Ag-NPs (to enroll SPR). To the best of our knowledge, this is being performed for the first time. Furthermore, we also report (as well for the first time) the design and clue characteristics of RL based on the plasmonic effect using this fiber. Namely, we managed to construct a fiber bearing an on-tip, specially prepared microsphere (microcavity). The idea behind this design was to utilize its unique advantage: a combination of the pronounced fluorescence in the visible (VIS) range at a properly chosen pump wavelength (given the presence of BAC with characteristic spectral bands) and the SPR phenomenon (given the presence of Bi-NPs/Ag-NPs). Additionally, the fiber exhibits low loss in VIS/NIR. As a result, we present a small-sized, low-threshold, 807 nm (under 532 nm pumping) RFL, for the first time. Note that the described approach offers a roadmap to manufacture similar RFLs in a very simple way.

2. Materials and Methods

For our studies, we used BAYAg (Bi/Al/Y/Ag co-doped) optical fiber for the proposed device report below. The raw chemical materials utilized in its fabrication are as follows:

$$1.5(\mathrm{M})\mathrm{Al}(\mathrm{NO_3})_3 + 0.5(\mathrm{M})\mathrm{AgNO_3} + 0.1(\mathrm{M})\mathrm{Bi}(\mathrm{NO_3})_3 + 0.2(\mathrm{M})\mathrm{Y}(\mathrm{NO_3})_3, \quad (1)$$

where M stands for moles.

The following is the procedure for the fabrication of the fiber.

A Bi/Al/Y/Ag co-doped silica-based optical preform was made through the standard Modified Chemical Vapor Deposition (MCVD) method in combination with the solution-doping technique. In the MCVD process, a single porous un-sintered SiO_2 soot layer was deposited onto the inner wall of a silica glass tube with outer/inner diameters of 20/17 mm at 1520 ± 5 °C. After complete deposition of the porous silica layer, solution doping was performed using an aqueous solution of the mixture according to (1) plus ~5% HNO_3 for ~1 h (HNO_3 was used to stop the formation of colloidal $BiONO_3$, spontaneously appearing during the preparation of $Bi(NO_3)_3$ solution at pH~7). A special setup was used for pouring the solution into the tube at a uniform rate to diminish imperfections and concentration variations along the preform length. The draining rate of the solution was controlled after dipping. It was observed that after 1 h of soaking an equilibrium was established between the chemical potential of ions, present both in the solution and within the porous layer. Therefore, almost all the pores were saturated by the various dopants, entered from the solution phase. After soaking, the solution was drained from the inner portion of the tube and the solvent was removed from the pores under a flow of N_2 gas for ~30 min at room temperature. Oxidation was performed at a temperature between 800 and 1000 °C in the presence of excessive O_2 for conversion of the nitrate salts present in the pores into corresponding oxides (Bi_2O_3, Al_2O_3, Ag_2O, and Y_2O_3). During the oxidation step, the temperature was adjusted in such a way that no sintering could take place, otherwise some OH- ions might be trapped within the porous layer. After oxidation, dehydration was carried out by properly selecting the temperature, Cl_2:O_2 ratio, and time. The period of dehydration was important for the reduction in OH content in the core glass. Dehydration

temperature was carried out at 900 °C with a Cl_2:O_2 ratio of 1.5:1 for ~30 min. After this, sintering of the soaked layer was performed by increasing the temperature from 1300 to 1800 °C until the core layer became transparent. In the last step, collapsing of the tube was performed in 3 passes of the burner at temperatures above 2000 °C. The burner traverse speed was decreased gradually from 5 to 1 cm/min in subsequent passes and finally, the solid silica glass-based optical preform with 10 mm diameter was obtained. An optical fiber of 125 μm diameter was drawn from the preform using a fiber drawing tower with an online resin coating with a thickness of 62.5 μm.

The fiber's core diameter and N.A. were measured as 12.6 μm and 0.19, respectively. The fiber is strongly multimode within the entire VIS-NIR range as its cutoff wavelength is ~3.14 μm. Its absorption and fluorescence spectra (at ~10 mW excitation using a fibered laser diode (LD) emitting at 406 nm) for two lengths are shown in Figure 1a,b, respectively; the cross-sectional image of the fiber at white-light illumination is in the inset of Figure 1a. One can reveal from the spectra that there are contributions in the fiber's absorption/fluorescence stemming from doping with Bi (Bi^0 or/and its agglomerates, e.g., NPs, and Bi-Al BAC (see, e.g., [24,36,37]) and Ag (presumably entering the fiber core in the form of Ag-NPs) (see, e.g., [19]).

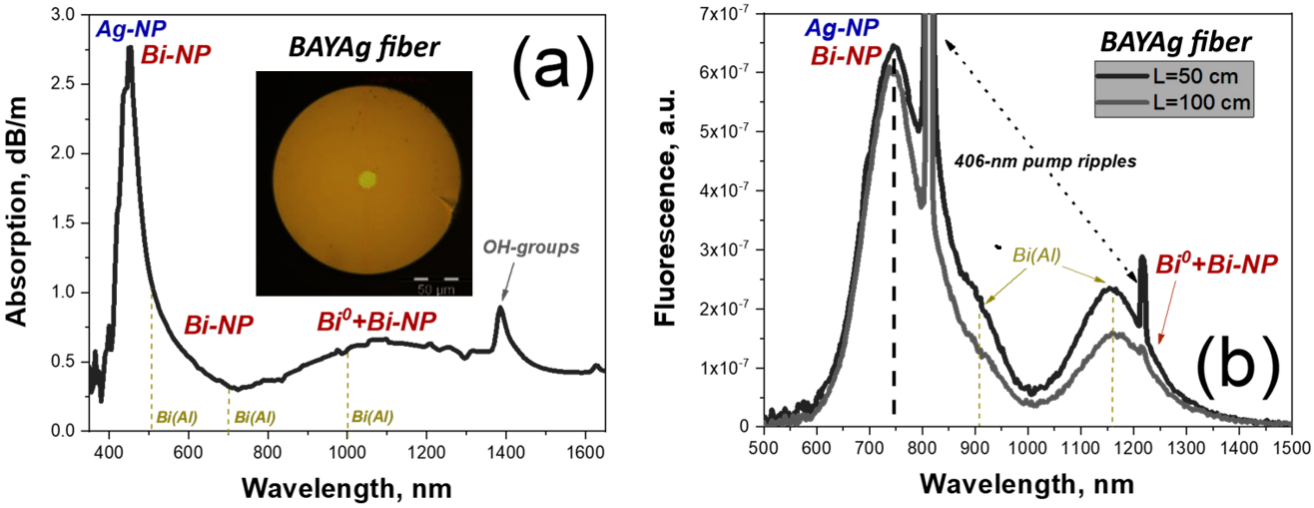


Figure 1. (**a**) Absorption and (**b**) fluorescence spectra of BAYAg fiber. Inset in (**a**)—microphotograph of its cleaved end at WL illumination.

In Figure 2a, we report the X-ray energy dispersive spectroscopy (EDS) of the fiber, which was obtained using a scanning electron microscope (Jeol model JSM-7800F, Peabody, MA, USA). The results show the presence of Bi, Ag, O, Al, and Si species in the fiber's core area. Note that the most pronounced peaks corresponding to Bi and Ag are grouped in Figure 2a from ~2.3 to ~3.4 keV, so it is natural to consider that their sources are NPs comprising both Bi and Ag species. Furthermore, since the core of the fiber was fabricated using the composition (1) at a high temperature (~2000 °C), the starter Ag/Bi-containing compounds 0.5(M) $AgNO_3$ + 0.1(M) $Bi(NO_3)_3$ should fade during the fabrication, leading to the following two basic effects: (*a*) the thermal decomposition of $AgNO_3$ and $Bi(NO_3)_3$ according to the reactions: $2AgNO_3 \rightarrow 2Ag\text{-NPs(solid)} + 2NO_2(gas) + O_2(gas)$ and $2Bi(NO_3)_3 \rightarrow 2Bi\text{-NPs(solid)} + 9O_2(gas) + 3N_2(gas)$ and (*b*) formation of metallic Bi^0 and/or clusters $(Bi_n)^0$ as well as Bi-NPs via a redox reaction [38–41]. Thus, the final fiber is expected to contain Bi-NPs, Ag-NPs, and probably 'hybrid' Bi/Ag-NPs [18].

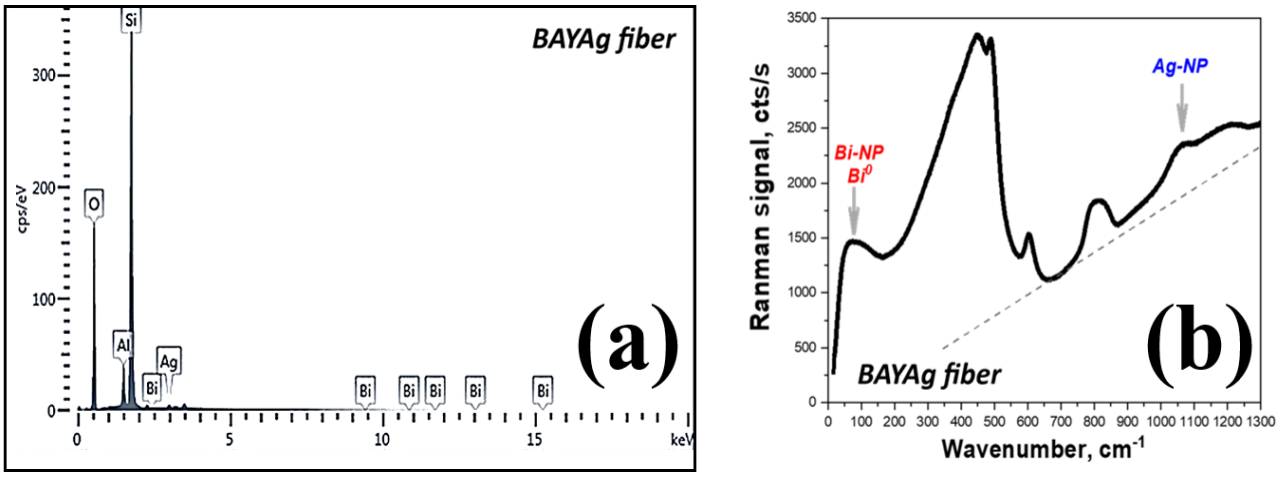


Figure 2. (**a**) X-ray ED spectrum for BAYAg fiber and (**b**) its Raman spectrum.

In Figure 2b, we present the Raman response of BAYAg fiber; it was obtained via the standard technique adapted to optical fiber. The excitation wavelength in this case was 514 nm (i.e., close to the pump at 532 nm, in the main-course experiments, reported below). In the experiment, we used a short-focus objective (50×) launching the pump light into the fiber. An analysis of the Raman spectrum revealed the following: (*a*) the studied fiber shows strong fluorescence, observed as a steep rise in the detected signal at increasing wavenumber (guided to the eye by the dashed gray line), which is confirmed by our experiments on fluorescence/lasing at 532 nm pumping; and (*b*) the pronounced peak in the spectrum at 50, . . . , 150 cm^{-1} evidence a notable contribution from the Bi-NPs and Bi^0 species (both Raman active in this range) while the peak near 1050 cm^{-1}, also expressed, indicates the presence of Ag-NPs [18] (both features are highlighted by gray arrows in Figure 2b).

Additionally, no detrimental effect upon the BAYAg fiber's mechanical properties was observed, which is due to the presence of very minor amounts of Ag, Bi, and Y; the oxides' contents were ~0.03, ~0.05, and ~1.25 wt.%, respectively, evaluated from the electron probe micro analyses (EPMA). Only Al_2O_3 content was relatively large (~5.0 wt.%) but, according to our earlier experience in making similar (co-doped with Bi/Al but Ag-free) fibers), it wouldn't lead to any brittleness or fragile behavior of the final Bi/Al/Y/Ag fiber.

3. Results

A 10 cm long piece of the fiber was placed in a fusion splicing machine (FSM-100 Arc Master Fujikura, Japan), specifically programmed for making a microsphere on the tip of one of the fiber's ends. A sketch of the machine's program, utilized for making a microsphere-on-fiber-tip unit, is demonstrated in Figure 3.

The resulting component can be addressed as a nearly spherical (slightly elliptical) cavity with a radius of ~300 μm. In Figure 4a, we show a schematized view of our RFL based on the design described above. The light from a pump laser (a fiberized LD at "green" wavelength) was launched through the splice into the fiber from the side opposite to the one where the microsphere was manufactured, so it first propagated along the entire fiber length and then within the microsphere, interacting with the dopants and igniting down-converted emission, the spectrum of which is in the orange–yellow region.

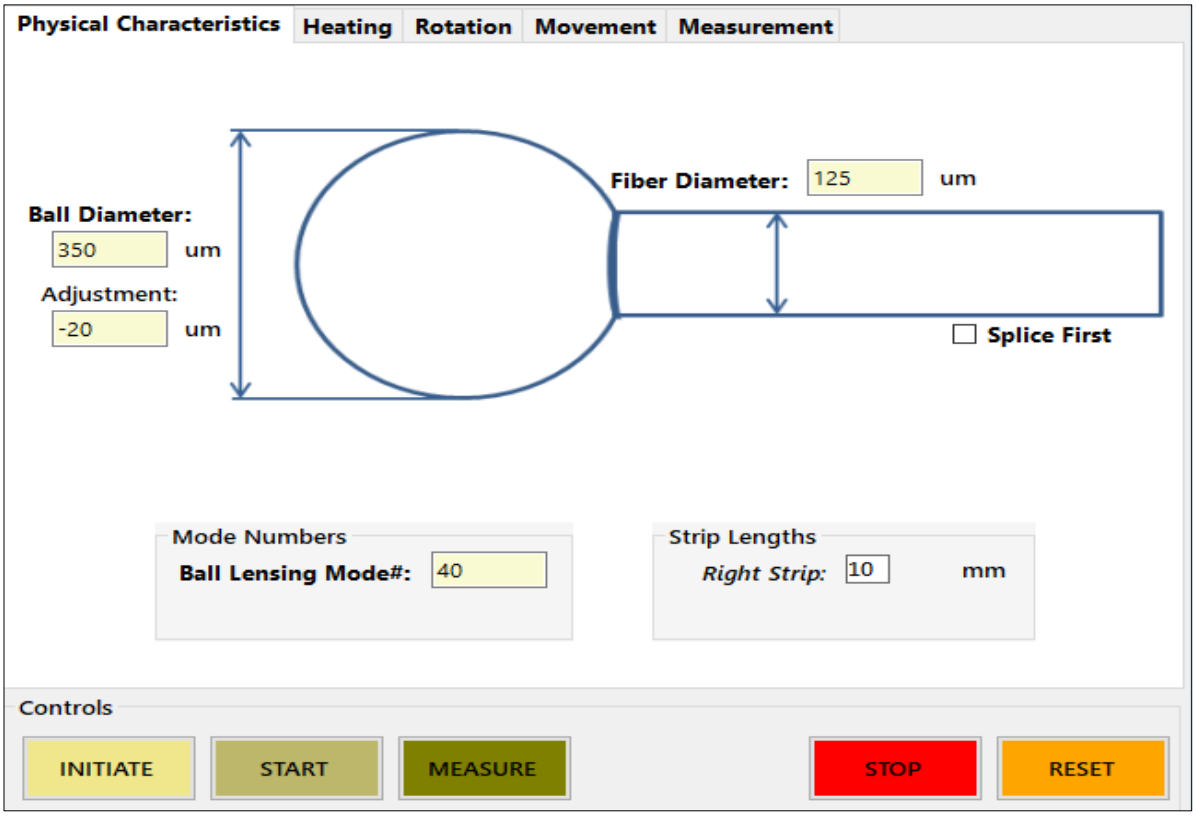


Figure 3. Programming a make-up of microsphere-on-fiber-tip structure using FSM.

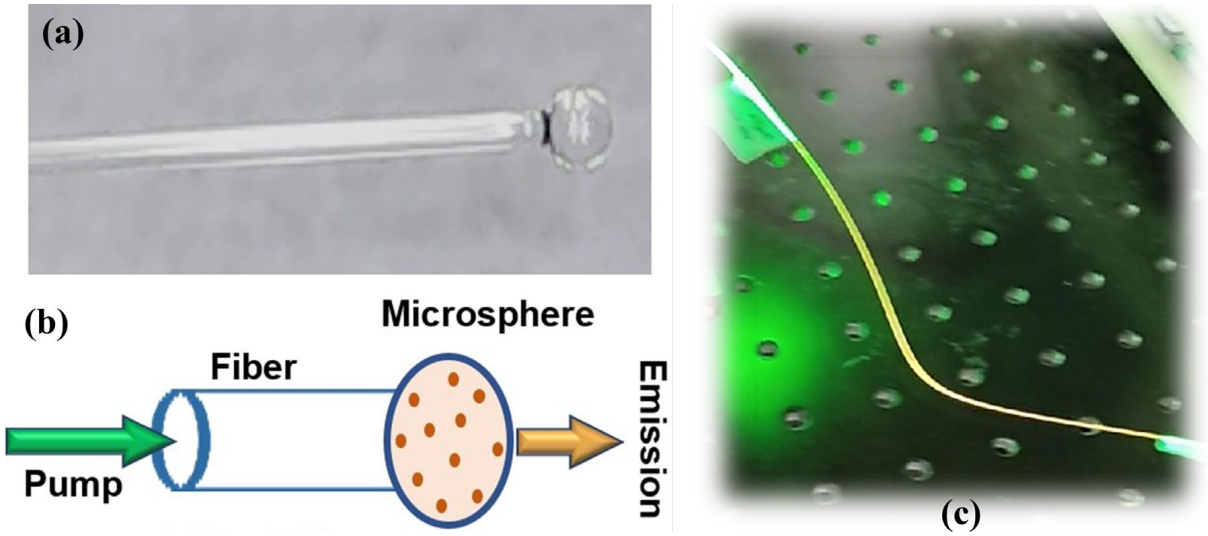


Figure 4. (**a**) Lateral view of the optical microscopy image of the microcavity on BAYAg fiber tip; (**b**) scheme of the plasmonic RFL based on microcavity-tipped BAYAg fiber; (**c**) fluorescence image of the fiber (without a microsphere on tip), pumped by 532 nm LD.

Note that the emission in our case is born within the microcavity, at the farthest part where the pump light enters and is well directional (highlighted by the arrow in Figure 4b), which could be seen by the naked eye. The outside 'lightening' of our setup when the pump power is set close to the laser threshold. Thus, the microsphere in our case functions simultaneously in two ways: on the one hand, it is of adequate size to be capable of producing the energy density inside it high enough for the 3D-plasmonic feedback mechanism to occur; and, on the other hand, the tip of the microcavity acts as a lens, guiding the emitted radiation along the axis of the optical fiber. As shown in Figure 4c,

the green light (at 532 nm) comes from the pumping LD, and the orange light is born in the fiber, presumably produced by the combined fluorescence of Ag-NPs and Bi(Al) BAC (see Figure 1b).

The measurements were performed with an Ando AQ-6312B optical spectrum analyzer, set to a spectral resolution of 0.05 nm. To examine the developed fiber-microcavity system, we pumped it using a standard fibered LD at 532 nm; launched into the BAYAg fiber pump power was limited to ~10 mW. The results are demonstrated in Figures 5–7.

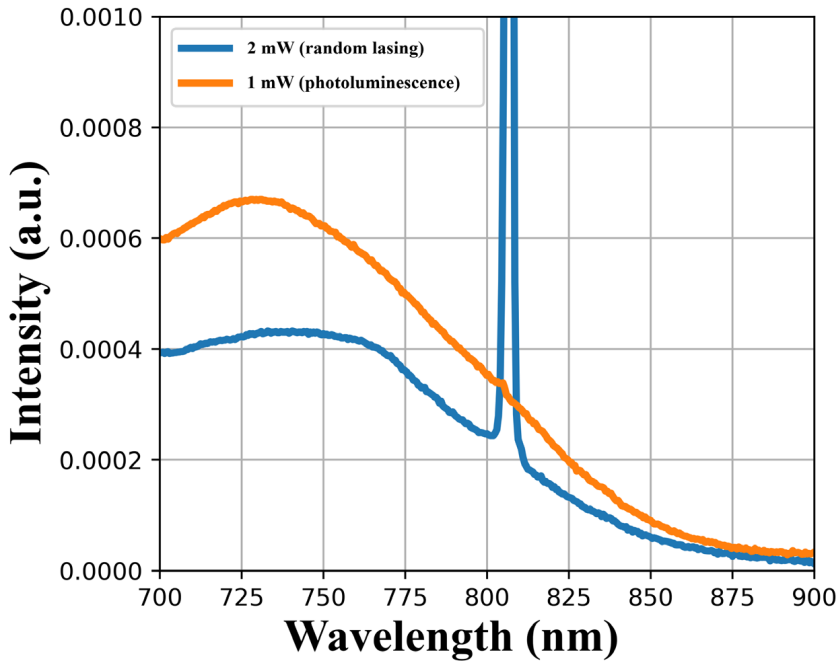


Figure 5. Transience from fluorescence (orange curve) to lasing (blue curve) around the threshold.

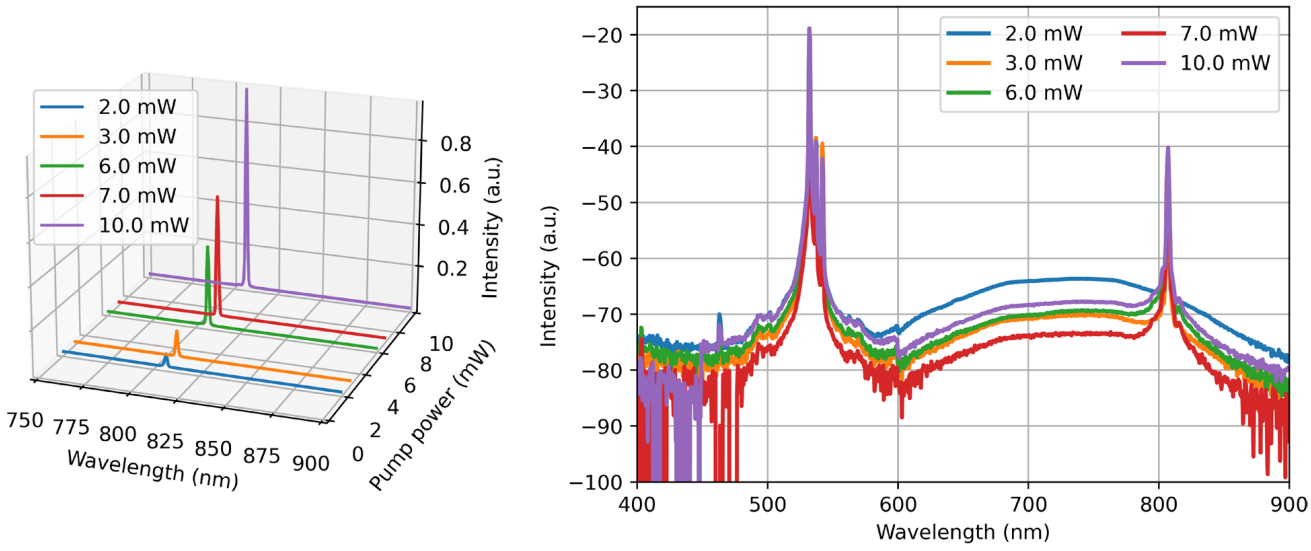


Figure 6. Plasmonic RL-emission at 807 nm: optical spectra recorded at variable pump power, launched into BAYAg fiber: on (**left**)—"3D" view of the laser line (linear scaling); on (**right**)—'common' "2D" spectra (logarithmic scaling), extended for showing the pump-light.

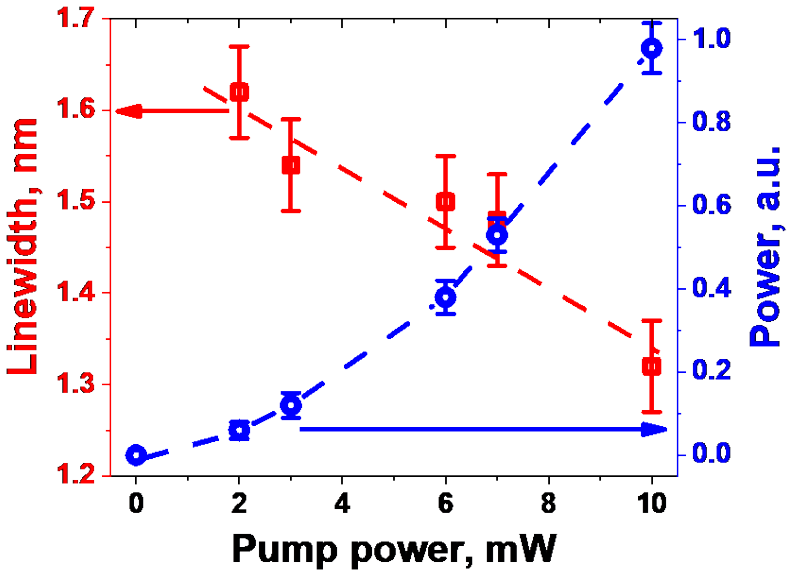


Figure 7. Power (right axis) and line FWHM (left axis): 807 nm lasing in function of 532 nm pump power.

Figure 5 shows the spectral behavior of the system at passing through the laser threshold. The figure clearly shows an abrupt transformation of the optical spectrum from the spectrally smooth fluorescence centered at ~730 nm (see the orange spectrum, captured at pump power of ~1.5 mW) to the narrow-line (~1.5 nm in FWHM) lasing at ~807 nm (see the blue spectrum, captured at pump power of ~2.0 mW). First, note the tremendously growing laser line's amplitude after passing the threshold and the simultaneously occurring depression of the remnant broadband fluorescence on its background, which is apparent from a comparison of the two spectra. This behavior appears to provide strong evidence for true lasing to arise in the system. Second, note that the drawn effect of the self-started lasing never happened when we attempted using 'naked' BAYAg fiber (i.e., without a microsphere on-tip); this proves the key role of the microsphere as an essential device element providing RL in our case. Third, note that remained "under-threshold" orange fluorescence (refer to the orange curve in Figure 5) itself is spectrally narrower than the one shown in Figure 1b; this shows that it is mainly produced in the microcavity, in the effect of whispery modes developing inside the latter.

Figure 6 demonstrates the laser spectra measured at the system output. For all 532 nm pump powers explored (up to 10 mW), the narrow-line (~1.6, . . ., 1.3 nm in FWHM) light at the unchanged central wavelength (807 nm) with steadily growing (at increasing the pump) amplitude is generated. The power and the FWHM of the output laser light in the function of the pump power are presented in Figure 7. The behavior of the output power vs. pump power (nonlinear growth) is typical for laser action; accordingly, linewidth steadily decreases at increasing pump power.

4. Discussion

The reported experimental data clearly reveals the achievement of the laser emission mentioned. The scenario for the obtainment of this result can be qualitatively explained as follows: The way we approach the phenomenon comprises, with adaptations required for the case of Bi as an emission-active species, the plasmonic effect, the energy transfer among Ag/Bi co-dopants, and the feedback of untrivial kind. We emphasize that the approach employed here is essentially combinative, where both co-doping of our Bi/Al/Y fiber with Ag NPs and the use of a microsphere as a microcavity proved that no RL arises using either as-fabricated Ag-free Bi/Al/Y fiber or, as mentioned Figure 5, using pieces of 'naked' BAYAg fiber (not covered by a microsphere).

In this regard, different authors shared evidence that the addition of silver can lead to improved luminescence properties of a material, for example, based on rare earths [25–35]. A similar phenomenon was uncovered by C. Van der Horst et al. [19] for Bi who performed a study on the synthesis and characterization of Bi-NPs/Ag-NPs in glasses, which particularly reports the absorption spectrum of the material in the UV-VIS region where characteristic absorption peaks of both kinds of NPs are observed. Furthermore, it ought to be remarked that the plasmonic resonances of Ag-NPs and Bi-NPs overlap and that the resulting spectrum limits the possibility of reabsorption of the fluorescence emitted by Bi(Al) BAC (and/or B^0 and its agglomerates) [24,36–39].

Furthermore, regarding our current realization of the fiber-based RL, we consider that the plasmon enhances the absorption at the pump wavelength (532 nm), which has the effect of reducing the threshold power for lasing at 807 nm and enlarges the field in the nearby Bi(Al) BAC (or B^0-related species); presumably, those effects are responsible of the orange emission that ultimately results in lasing [42].

It deserves mentioning that, formally, no 'common' feedback amplification is provided in our case to generate the laser light but instead, as explained by De Matos et al. [2], "the optical plasmonic feedback (Bi-NPs/Ag-NPs) in the random laser is provided within the amplifying medium by random light paths that result in an increased emission intensity and reduced line width" which partly explains our main results. Furthermore, we must highlight the crucial role that the microcavity plays in the form of a microsphere on the fiber's tip. The microcavities provide strong light confinement and scattering that ultimately lead to and facilitate RL [43].

We emphasize that our current study adheres to the already formed trend of exploiting the plasmonic effect itself and, particularly, doping optical fibers with Ag, towards such contemporary applications in fiber photonics as nonlinear broadband modulation and passive Q-switching in fiber lasers [44,45], generating vortex beams [46], etc.

5. Conclusions

The data reported in this paper allow the following conclusions to be made. The superposition of the SPR at Ag-NPs/Bi-NPs, the fluorescence spectrum of the Bi active centers, namely of Bi(Al) type, and the geometry used (viz., the microcavity on the fiber's tip, responsible for effective feedback), are grounds for the reported narrow-linewidth, low-threshold lasing system we reported. We have shown that (*a*) Ag/Bi NPs in-pair with Bi(Al) active centers in the BAYAg fiber are the clue factors behind random lasing obtained; (*b*) the microcavity (microsphere on the fiber's tip) is a prerequisite for enrolling the high-intensity and high-directionality of the laser light outcoming from the system. Compared to others, our RFL design is easily feasible and robust.

Author Contributions: Conceptualization, M.A.M.G., J.L.L.M., A.V.K. and M.C.P.; methodology, M.A.M.G. and J.L.L.M.; formal analysis, M.A.M.G., J.L.L.M., A.V.K. and K.G.H.C.; investigation, J.A.d.l.F.L., M.A.M.G., A.V.K., K.G.H.C. and M.C.P.; writing—original draft preparation, M.A.M.G., J.L.L.M. and A.V.K.; writing—review and editing, A.V.K. and M.A.M.G. All authors have read and agreed to the published version of the manuscript.

Funding: J.L.L.M. acknowledges financial support from the Universidad de Guanajuato (Mexico) through the CIIC 2024-proyecto 043/2024.

Data Availability Statement: The data are available upon request to the corresponding author.

Acknowledgments: J.A.F.L. is grateful for the CONAHCyT (Mexico) scholarship to pursue doctoral studies.

Conflicts of Interest: The authors declare no conflicts of interest.

References

1. Lawandy, N.M.; Balachandran, R.M.; Gomes, A.S.L.; Sauvain, E. Laser action in strongly scattering media. *Nature* **1994**, *368*, 436–438. [CrossRef]
2. de Matos, C.J.; Menezes, L.D.S.; Brito-Silva, A.M.; Martinez Gámez, M.A.; Gomes, A.S.; de Araújo, C.B. Random fiber laser. *Phys. Rev. Lett.* **2007**, *99*, 153903. [CrossRef] [PubMed]
3. Frolov, S.; Gellermann, W.; Ozaki, M.; Yoshino, K.; Vardeny, Z. Cooperative emission in π-conjugated polymer thin films. *Phys. Rev. Lett.* **1997**, *78*, 729. [CrossRef]
4. Dice, G.D.; Mujumdar, S.; Elezzabi, A.Y. Plasmonically enhanced diffusive and subdiffusive metal nanoparticle-dye random laser. *Appl. Phys. Lett.* **2005**, *86*, 131105. [CrossRef]
5. Chang, S.-W.; Liao, W.-C.; Liao, Y.-M.; Lin, H.-I.; Lin, H.-Y.; Lin, W.-J.; Lin, S.-Y.; Perumal, P.; Haider, G.; Tai, C.-T.; et al. A white random laser. *Sci. Rep.* **2018**, *8*, 2720. [CrossRef]
6. Parola, S.; Julián-López, B.; Carlos, L.D.; Sanchez, C. Optical properties of hybrid organic-inorganic materials and their applications. *Adv. Funct. Mater.* **2016**, *26*, 6506–6544. [CrossRef]
7. Sapienza, R. Determining random lasing action. *Nat. Rev. Phys.* **2019**, *1*, 690–695. [CrossRef]
8. Luan, F.; Gu, B.; Gomes, A.S.; Yong, K.-T.; Wen, S.; Prasad, P.N. Lasing in nanocomposite random media. *Nano Today* **2015**, *10*, 168–192. [CrossRef]
9. Cao, H. Review on latest developments in random lasers with coherent feedback. *J. Phys. A Math. Gen.* **2005**, *38*, 10497–10535. [CrossRef]
10. Meng, X.; Fujita, K.; Murai, S.; Matoba, T.; Tanaka, K. Plasmonically controlled lasing resonance with metallic-dielectric core shell nanoparticles. *Nano Lett.* **2011**, *11*, 1374–1378. [CrossRef]
11. Redding, B.; Choma, M.A.; Cao, H. Speckle-free laser imaging using random laser illumination. *Nat. Photonics* **2012**, *6*, 355–359. [CrossRef] [PubMed]
12. Cui, L.; Shi, J.; Wang, Y.; Zheng, R.; Chen, X.; Gong, W.; Liu, D. Retrieval of contaminated information using random lasers. *Appl. Phys. Lett.* **2015**, *106*, 201101. [CrossRef]
13. Churkin, D.V.; Sugavanam, S.; Vatnik, I.D.; Wang, Z.; Podivilov, E.V.; Babin, S.A.; Rao, Y.; Turitsyn, S.K. Recent advances in fundamentals and applications of random fiber lasers. *Adv. Opt. Photonics* **2015**, *7*, 516–569. [CrossRef]
14. Wang, Y.; Duan, Z.; Qiu, Z.; Zhang, P.; Wu, J.; Zhang, D.; Xiang, T. Random lasing in human tissues embedded with organic dyes for cancer diagnosis. *Sci. Rep.* **2017**, *7*, 8385. [CrossRef] [PubMed]
15. Ma, R.; Rao, Y.J.; Zhang, W.L.; Hu, B. Multimode random fiber laser for speckle-free imaging. *IEEE J. Sel. Top. Quantum Electron.* **2018**, *25*, 1–6. [CrossRef]
16. Mermillod-Blondin, A.; Mentzel, H.; Rosenfeld, A. Time-resolved microscopy with random lasers. *Opt. Lett.* **2013**, *38*, 4112–4115. [CrossRef]
17. Han, B.; Cheng, Q.; Tao, Y.; Ma, Y.; Liang, H.; Ma, R.; Qi, Y.; Zhao, Y.; Wang, Z.; Wu, H. Spectral manipulations of random fiber lasers: Principles, characteristics, and applications. *Laser Photonics Rev.* **2024**, *18*, 2400122. [CrossRef]
18. Toudert, J.; Serna, R.; Jimenez de Castro, M. Exploring the optical potential of nano-bismuth: Tunable surface plasmon resonances in the near ultraviolet-to-near infrared range. *J. Phys. Chem. C* **2012**, *116*, 20530–20539. [CrossRef]
19. Van der Horst, C.; Silwana, B.; Iwuoha, E.; Somerset, V. Synthesis and characterization of Bismuth-Silver nanoparticles for electrochemical sensor applications. *Anal. Lett.* **2015**, *48*, 1311–1332. [CrossRef]
20. Hutter, E.; Fendler, J.H. Exploitation of localized surface plasmon resonance. *Adv. Mater.* **2004**, *16*, 1685–1706. [CrossRef]
21. Petryayeva, E.; Krull, U.J. Localized surface plasmon resonance: Nanostructures, bioassays and biosensing—A review. *Anal. Chim. Acta* **2011**, *706*, 8–24. [CrossRef] [PubMed]
22. Firstov, S.V.; Khegai, A.M.; Kharakhordin, A.V.; Alyshev, S.V.; Firstova, E.G.; Ososkov, Y.J.; Melkumov, M.A.; Iskhakova, L.D.; Evlampieva, E.B.; Lobanov, A.S.; et al. Compact and efficient o-band bismuth-doped phosphosilicate fiber amplifier for fiber-optic communications. *Sci. Rep.* **2020**, *10*, 11347. [CrossRef] [PubMed]
23. Vakhrushev, A.; Umnikov, A.; Lobanov, A.; Firstova, E.G.; Evlampieva, E.B.; Riumkin, K.; Alyshev, A.V.; Khegai, A.; Guryanov, A.; Iskhakova, L.D.; et al. W-type and graded-index bismuth-doped fibers for efficient lasers and amplifiers operating in E-band. *Opt. Express* **2022**, *30*, 1490–1498. [CrossRef] [PubMed]
24. Khegai, A.; Alyshev, S.; Vakhrushev, A.; Riumkin, K.; Umnikov, A.; Firstov, S. Recent advances in Bi-doped silica-based optical fibers: A short review. *J. Non-Cryst. Solids X* **2022**, *16*, 100126. [CrossRef]
25. Hernandez, M.A.V.; Martinez Gámez, M.A.; Martínez, J.L.L.; Kir'yanov, A.V. Enhanced near-infrared emission from holmium-ytterbium co-doped phosphate glasses containing silver nanoparticles. *Appl. Spectrosc.* **2014**, *68*, 1247–1253. [CrossRef]
26. Vallejo Hernandez, M.; Martinez Gámez, M.A.; Kir'yanov, A.; Martinez, J. Optical properties of phosphate glasses co-doped with Yb^{3+} and silver nanoparticles. *Chin. Phys. B* **2014**, *23*, 124214.

27. Vijayakumar, R.; Nagaraj, R.; Suthanthirakumar, P.; Karthikeyan, P.; Marimuthu, K. Silver (Ag) nanoparticles enhanced luminescence properties of Dy^{3+} ions in borotellurite glasses for white light applications. *Spectrochim. Acta Part A Mol. Biomol. Spectrosc.* **2018**, *204*, 537–547. [CrossRef]
28. Vijayakumar, R.; Marimuthu, K. Luminescence studies on Ag nanoparticles embedded Eu^{3+} doped boro-phosphate glasses. *J. Alloys Compd.* **2016**, *665*, 294–303. [CrossRef]
29. Bae, C.-H.; Lim, K.-S. Enhanced visible emission in Eu^{3+} doped glass containing Ag-clusters, Ag nanoparticles, and ZnO nanocrystals. *J. Alloys Compd.* **2019**, *793*, 410–417. [CrossRef]
30. Pan, Z.; Ueda, A.; Aga, R., Jr.; Burger, A.; Mu, R.; Morgan, S. Spectroscopic studies of Er^{3+} doped Ge-Ga-S glass containing silver nanoparticles. *J. Non-Cryst. Solids* **2010**, *356*, 1097–1101. [CrossRef]
31. Cheng, P.; Zhou, Y.; Su, X.E.; Zhou, M.; Zhou, Z. The near-infrared band luminescence in silver NPs embedded tellurite glass doped with $Er^{3+}/Tm^{3+}/Yb^{3+}$ ions. *J. Alloys Compd.* **2017**, *714*, 370–380. [CrossRef]
32. Zhao, G.; Xu, L.; Meng, S.; Du, C.; Hou, J.; Liu, Y.; Guo, Y.; Fang, Y.; Liao, M.; Zou, J.; et al. Facile preparation of plasmon enhanced near-infrared photoluminescence of Er^{3+} doped Bi_2O_3-B_2O_3-S_iO_2 glass for optical fiber amplifier. *J. Lumin.* **2019**, *206*, 164–168. [CrossRef]
33. Swetha, B.; Keshavamurthy, K.; Jagannath, G. Influence of size of ag np on spectroscopic performances of Eu^{3+} ions in sodium borate glass host. *Optik* **2021**, *240*, 166918. [CrossRef]
34. Kindrat, I.I.; Padlyak, B.V.; Lisiecki, R.; Drzewiecki, A.; Adamiv, V.T. Effect of silver co-doping on luminescence of the Pr^{3+}-doped lithium tetraborate glass. *J. Lumin.* **2022**, *241*, 118468. [CrossRef]
35. Dan, H.K.; Trung, N.D.; Tam, N.M.; Ha, L.T.; Lien, T.K.; Thai, N.L.; Zhou, D.; Qiu, J. The effect of Al^{3+} ions on the self-reduction process of Yb^{3+} to Yb^{2+} ions and optical properties of Nd^{3+}/Yb^{n+} (n = 3, 2) co-doped transparent silicate glass-ceramics containing Ba_2LaF_7 nanocrystals and Ag nanoparticles. *Ceram. Int.* **2024**, *50*, 25412–25421. [CrossRef]
36. Bufetov, I.A.; Melkumov, M.A.; Firstov, S.V.; Riumkin, K.E.; Shubin, A.V.; Khopin, V.F.; Guryanov, A.N.; Dianov, E.M. Bi-doped optical fibers and fiber lasers. *IEEE J. Select. Top. Quant. Electron.* **2014**, *20*, 0903815. [CrossRef]
37. Dianov, E.; Melkumov, M.; Firstov, S. Bismuth-doped fibre lasers and optical amplifiers. In *Handbook of Laser Technology and Applications*; CRC Press: Boca Raton, FL, USA, 2021; pp. 535–556.
38. Khonthon, S.; Morimoto, S.; Arai, Y.; Ohishi, Y. Redox equilibrium and NIR luminescence of Bi_2O_3-containing glasses. *Opt. Mater.* **2009**, *31*, 1262–1268. [CrossRef]
39. Peng, M.; Zollfrank, C.; Wondraczek, L. Origin of broad NIR photoluminescence in bismuthate glass and Bi-doped glasses at room temperature. *J. Phys. Condens. Matter* **2009**, *21*, 285106. [CrossRef]
40. Singh, S.P.; Karmakar, B. Single-step synthesis and surface plasmons of bismuth-coated spherical to hexagonal silver nanoparticles in dichroic Ag: Bismuth glass nanocomposites. *Plasmonics* **2011**, *6*, 457–467. [CrossRef]
41. Halder, A.; Kir'yanov, A.V.; Barmenkov, Y.O.; Sekiya, E.H.; Saito, K. Discussion on Raleigh scattering as a dominant loss factor in VIS/NIR in bismuth-doped silicate fibers [invited]. *Opt. Mater. Express* **2019**, *9*, 2817–2827.
42. Krishnan, M.L.; Neethish, M.; Kumar, V.R.K.; Vendamani, V.; Devi, K.D.; Mohan, D.B.; Nandhagopal, P.; Behera, N. Photoluminescence & structural studies of Ag: Alkali bismuth silicate glasses. *Optik* **2023**, *273*, 170474.
43. Zhu, H.; He, Z.; Wang, J.; Zhang, W.; Pei, C.; Ma, R.; Zhang, J.; Wei, J.; Liu, W. Microcavity complex lasers: From order to disorder. *Ann. Phys.* **2024**, *536*, 2400112. [CrossRef]
44. Sun, J.; Cheng, H.; Xu, L.; Fu, B.; Liu, X.; Zhang, H. Ag/MXene composite as a broadband nonlinear modulator for ultrafast photonics. *ACS Photonics* **2023**, *10*, 3133–3142. [CrossRef]
45. Zhao, X.; Sun, J.; Wang, Y.; Wang, X.; Fu, B. Ag/MXene as saturable absorber for Tm:Ho co-doped Q-switched fiber laser. *Nanomaterials* **2024**, *14*, 951. [CrossRef]
46. Zhang, C.; Zhang, L.; Zhang, H.; Fu, B.; Wang, J.; Qiu, M. Pulsed polarized vortex beam enabled by metafiber lasers. *PhotoniX* **2024**, *5*, 36. [CrossRef]

Disclaimer/Publisher's Note: The statements, opinions and data contained in all publications are solely those of the individual author(s) and contributor(s) and not of MDPI and/or the editor(s). MDPI and/or the editor(s) disclaim responsibility for any injury to people or property resulting from any ideas, methods, instructions or products referred to in the content.